Atomic Energy, Vol. 104, No. 2, 2008

APPLICATION OF TWAC BEAMS FOR DIAGNOSTICS OF FAST PROCESSES

A. A. Golubev, V. S. Demidov,
E. V. Demidova, M. M. Kats,
S. B. Kolerov, V. S. Skachkov,
G. N. Smirnov, V. I. Turtikov,
A. D. Fertman, and B. Yu. Sharkov

UDC 539.12

The parameters of a TWAC accelerator–storage complex of an experimental facility for proton radiography of fast processes and static objects are presented. The time structure of the proton beam from the accelerator makes it possible to perform diagnostics of dynamic processes occurring at rates up to 20 km/sec. It is shown that the spatial resolution of the facility with respect to the sharp boundary of the density of an object with a thickness differential up to 4.5 g/cm^2 will be 8 μm with contrast ~0 .67.

The TWAC terawatt accelerator–storage complex possesses a wide spectrum of accelerated particles with respect to mass and energy [1, 2]. The proton accelerator in the complex is capable of generating intense beams of protons in a wide energy range. The proton beams are used for density diagnostics of a plasma target [3, 4]. Methods for measuring the density of a target with high spatial resolution using the proton radiography facility are now being developed.

Radiography as a method for transilluminating samples which are opaque to visible light for purposes of studying their internal structure has existed for a long time. Work on the application of a proton beam for radiography began in 1965 [5]. Images of the crystal lattices of many substances have been obtained using the shadow method in proton beams with energy up to 1 MeV. The prospects for developing proton radiography as a method of nondestructive flaw detection have been examined in [6]. The first experimental works on proton radiography appeared 50 years ago; proton radiography soon competed successfully with x-ray radiography in flaw detection, where high contrast sensitivity is required [7]. Moreover, ion beams are also finding application in radiography. For example, the first experiments in our country on radiography were performed in 2003 with 200 MeV/amu carbon ions at the Institute for Theoretical and Experimental Physics [8].

The possibilities of experiments performed according to the protons–object–detector scheme are limited by multiple scattering of protons in the object. The images obtained did not have a high contrast, and experiments were performed only on static objects. At the end of the 1990s, works which raised proton radiography to a much higher technological level were performed at the Nuclear Science Center LASCE in Los Alamos (USA). It was shown that the negative effects due to multiple scattering can be suppressed if a system of magnetic lenses is placed between the object and the detector [9]. It was shown that high contrast images of not only static but also rapidly changing dynamic objects can be obtained. The radiographic facility based on 800 MeV proton beams in LANSCE made it possible to obtain up to 30 frames of images of objects with density ranging from 0.05 to 50 g/cm^2, spatial resolution ~100–200 μm, frame exposure time ~100 nsec, and frame separation time up to 500 nsec.

Proton and x-ray radiography are the only currently used methods that yield direct information about the microstructure of a substance and the density distribution in a dynamic experiment. However, proton radiography surpasses x-ray radio-

State Science Center of the Russian Federation – Institute of Theoretical and Experimental Physics. Translated from Atomnaya Énergiya, Vol. 104, No. 2, pp. 99–106, February, 2008. Original article submitted October 2, 2007.

1063-4258/08/10402-0134

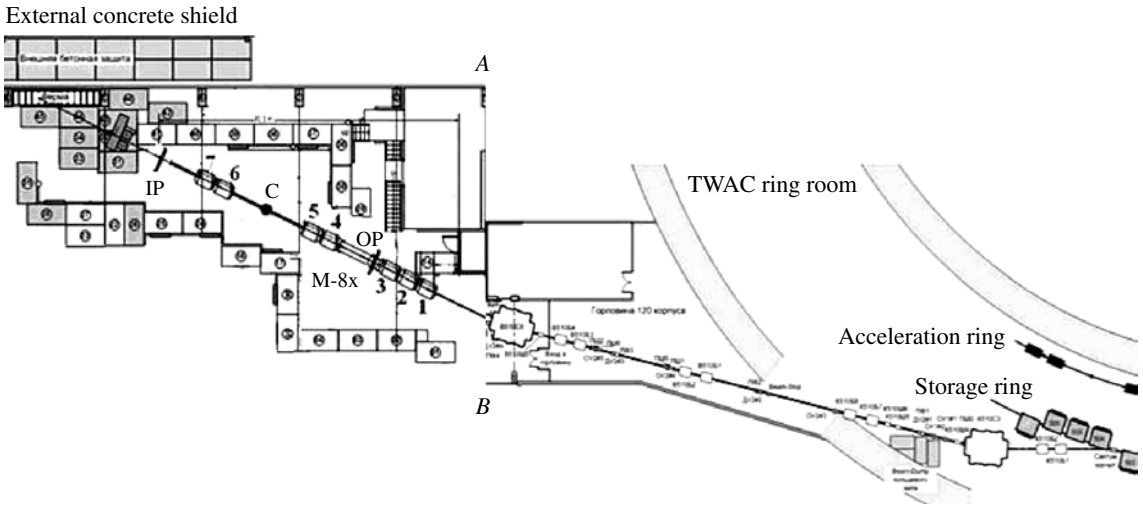

Fig. 1. Arrangement of the magnetic components, forming a proton beam for radiographic experiments, and quadrupole lenses of the proton radiography facility in the TWAC accelerator.

graphy with respect to many parameters: it has high spatial and temporal resolution as well as high transillumination power and permits recording images in a large dynamical range. In addition, the method permits multi-frame recording of dynamic processes, which makes it possible to follow the evolution of the state of a substance experimentally.

Facility for Proton Radiography at the Institute of Theoretical and Experimental Physics. One problem for a radiographic facility is investigating the physics of extreme states arising in matter, in particular, in explosive experiments. Work with explosives as an object of investigation requires an explosion chamber, which provides safety, for performing experiments. The effects of the shock wave due to the products of an explosion on the chamber wall are mitigated by evacuating the interior volume of the chamber. The chamber consists of a thick-wall spherical tank with windows which pass a proton beam and simultaneously protect the vacuum system of the accelerator from the products of the explosion. The experimental sample is placed inside the chamber and lies in the path of the proton beam.

Figure 1 displays the arrangement of the magnetic components and quadrupole lenses of the exit channel and the radiographic facility. The first part of the figure shows a part of the magnet room of the accelerator complex – the inner (acceleration) ring and the outer (storage) ring. Only the outer ring is used for proton radiography. Extraction is performed with a septum magnet. The line *A–B* separates the exit channel and the facility being developed. The scale to the left of this line is increased by a factor of 2.5. The exit channel is 63 m long and consists of two bending magnets and eight magnetic quadrupole lenses. A proton beam with momentum $p = 1.5$ GeV/sec ($\delta p/p = 0.1\%$), distributed uniformly along a 60 mm in diameter circle and having divergence 0.5 mrad, is formed at the channel exit. The intensity of the beam is $\sim 10^{11}$ protons per pulse. The standard duration of the proton beam is 800 nsec. The duration of each of the four proton beam pulses is 60 ± 5 nsec. The interval between pulses is 250 ± 15 nsec. Such a structure makes it possible to obtain during one cycle of the proton beam four proton radiographic pictures of the dynamic processes being studied. The sample chamber lies in the OP plane.

The magnetic optics in the facility consists of a system of magnetic quadrupole lenses (Nos. 1–7) whose purpose is to prepare the proton beam for transilluminating an object placed in the object plane OP and forms an image of the object in the image plane IP. The detection system consists of a scintillation converter, which converts the proton beam into a light image that can be recorded with a fast photographic camera.

The magnetic optics of the facility for proton radiography with image transmission coefficient −1 consists of seven quadrupole lenses of the type ML-15, which are 0.9 m long and have an aperture of 150 mm; the maximum field on a pole is 0.6 T. The direction of the fields in the quadrupoles alternates in the sequence FDFDFDF, where F and D denote focusing and defocusing of the proton beam by a quadrupole in the horizontal plane.

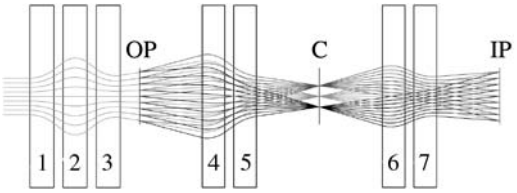

Fig. 2. Arrangement of the magnetic components and the course of the proton rays of the channel of the proton radiographic facility with image transmission coefficient −1.

A matching system consisting of lenses Nos. 1–3 serves to prepare the optimal parameters of the proton beam in the object plane OP and for partial compensation of the chromatic aberrations of the facility. The magnetic quadrupole lenses Nos. 4–7 with equal absolute fields (~0.258 T) comprise the measuring system of the facility. The plane OP and the measuring plane IP are arranged symmetrically with respect to the point C near which collimators and anticollimators will be positioned. The remaining part of the beam is utilized in the beam absorber, which consists of iron, lead, and paraffin. The radiation protection consisting of concrete blocks protects workers outside the confines of the shielding [10].

A proton microscope M with image magnification coefficient −8, employing magnetic quadrupole lenses based on permanent magnets consisting of a neodymium–iron–boron alloy, is placed behind the object plane OP.

The parameters of the magnetic optical facility are optimized using the COSY Infinity program [11]. The optimization results for a system with coefficient −1 are displayed in Fig. 2. The designations for the components of the facility are the same as in Fig. 1. The facility is 18.4 m long. For optimization, the requirement that the test objects be placed inside a 0.7 m in diameter explosive target chamber was taken into account. Standard collimators and anticollimators in the form of continuous rods oriented along the axis of the beam are placed in the C plane. For optimal operation of the collimators, the locations of the Fourier planes in the X and Y projections were required to coincide in this plane. Under this condition, protons which have acquired different multiple Coulomb scattering angles in the target are spatially separated in the C plane. For the proton trajectories shown in Fig. 2, the initial divergence of the beam is $\Delta\varphi = 0.5$ mrad. The divergence increases to 2 mrad beyond the OP plane, containing a 3 mm thick copper cylindrical object. The fact that the momentum of the protons beyond the OP plane decreases by 4% as a result of ionization losses in the object was taken into account when the trajectories were constructed. In a system initially tuned to momentum 1.5 GeV/sec, the image will be focused somewhat farther from the computed position of the detector. The magnetic field of the quadrupole lenses was adjusted to maintain the position of the detector. It was determined by computational means that the relative change of the magnetic field must equal the relative change of the proton momentum.

The resolving power of the facility with respect to a point emitter was evaluated analytically. To first order in the momentum spread $\Delta \equiv \delta p/p$ for a proton with initial coordinates (x, θ) in the object plane, the final coordinates in the image plane can be expressed as follows [12]:

$$x_f = R_{11}x + R_{12}\theta + R'_{11}x\Delta + R'_{12}\theta\Delta + R'_{12}\varphi\Delta + ..., \tag{1}$$

where R_{11}, R_{12}, R'_{11}, and R'_{12} are the matrix elements of the transport matrix, and φ is the rms value of the multiple Coulomb scattering angle in the experimental object. The effect of the factor $R'_{11}x\Delta + R'_{12}\theta\Delta$ from relation (1) on the resolution of the proton radiographic system can be eliminated by using a batching system which takes account of the angular correlation of the initial proton beam, where $\theta = wx$, $w = -R'_{11}/R'_{12}$, and $R_{12} = 0$ from the focusing condition. In this case, we shall rewrite expression (1) as

$$x_f = R_{11}x + R'_{12}\varphi\Delta + ... \tag{2}$$

Chromatic aberrations, which are described by the coefficients R'_{12}/R_{11}, where the matrix element R_{11} is numerically equal to the magnification of the optical system, make the main contribution to the smearing of the image of a point source.

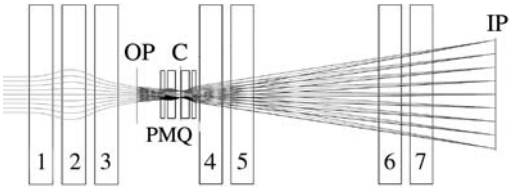

Fig. 3. Arrangement of the magnetic components and the proton trajectories in the channel of a proton radiographic facility with image transmission coefficient −8.

For the present system of quadrupole lenses $R_{11} = -1$ and $R_{12} = 0$, the image of the object is a mirror image and is inverted. The coefficient $R'_{12} = 11.32$ m is obtained by optimizing the system using the COSY Infinity program. Then the resolution of the system is given by the expression $\Delta x_f = R'_{12}\varphi\Delta$. For a 5 mm thick copper object ($\varphi = 3$ mrad, $\Delta = 0.0015$), $\Delta x_f \cong 51$ μm.

Figure 3 displays the results of optimizing the arrangements of the quadrupole lenses on permanent magnets in a proton microscope with eight-fold magnification. The geometric dimensions and number of the quadrupole lenses on permanent magnets were chosen from three conditions: they must be placed between the OP plane and the lens No. 4 (see Figs. 2 and 3), the possibility of installing an explosive target chamber must be preserved, and the coordinates of the measuring plane must remain the same. When optimizing with the COSY Infinity program, a system with four quadrupole lenses based on permanent magnets with the following parameters was chosen as initial data: the lenses are 0.16 and 0.32 mm long, the aperture is 40 mm, and the field on a pole is 0.6 T.

The optimal coordinates for the quadrupole lenses on permanent magnets and the currents in the quadrupole lenses Nos. 1–3 of the matching system where determined from the conditions where the image is focused in the IP plane and the spatial chromatic aberration effects are suppressed. Since quadrupole lenses based on permanent magnets are used in the proton microscope, the sharpness of the image will be tuned by changing their relative arrangement. The distance between the quadrupole lens No. 4 based on permanent magnets in the quadrupole ML-15 No. 4 remains unchanged and equal to 0.15 m; the relative arrangement of the remaining lenses is calculated for the corresponding proton momentum taking account of the ionization losses in the object. For momentum 1.5 GeV/sec, the distance between the quadrupoles Nos. 1–2 and 3–4 is 164 mm and the distance between Nos. 2–3 is 279.5 mm.

To estimate the spatial resolving power of the proton microscope with respect to a point emitter, the smearing of the image as a result of the extension of the object in the direction of the proton beam must be taken into account. For a microscope with eight-fold magnification, a displacement by 5 mm from the focal plane of the system is characterized by smearing of the image of the object by 200 μm. Thus, the error in the image plane for a 5 mm thick copper object will be ~50 μm; the value reduced to the scale of the object is 11 μm. We note that the resolution of the facility was obtained analytically taking account of the average values of the angles of multiple scattering, the proton energy losses to ionization of the medium, and fluctuations of these values.

Simulation of the Facility Using the GEANT Program. The results of the analytical estimate of the resolution were refined by numerical simulation of the magnetic optics system of the facility. The simulation was based on the program GEANT (version 3.21), which makes it possible not only to simulate all known types of interactions of elementary particles but also to follow the passage of the products of nuclear reactions to all components of the experimental setup, which in our case are quadrupole magnets, the experimental test objects, air gaps, the walls of vacuum tubes, and so forth. The geometric parameters of the facility are described in the program in a natural scale. Two variants of the programs were written: for magnification coefficients −1 and −8. Some subprograms, describing the spatial arrangement of the 11 quadrupole magnetic lenses and the arrangement of the object and image planes, were used in both variants. The variable parameters were the magnetic fields in the lenses ML-15 and the relative arrangement of the permanent-magnet lenses. The relative arrangement of the permanent-magnet lenses is used to determine the magnification factor of the microscope and to make an adjustment for the average energy of the protons after the object. The variants differed by the dimensions and granularity of the models of

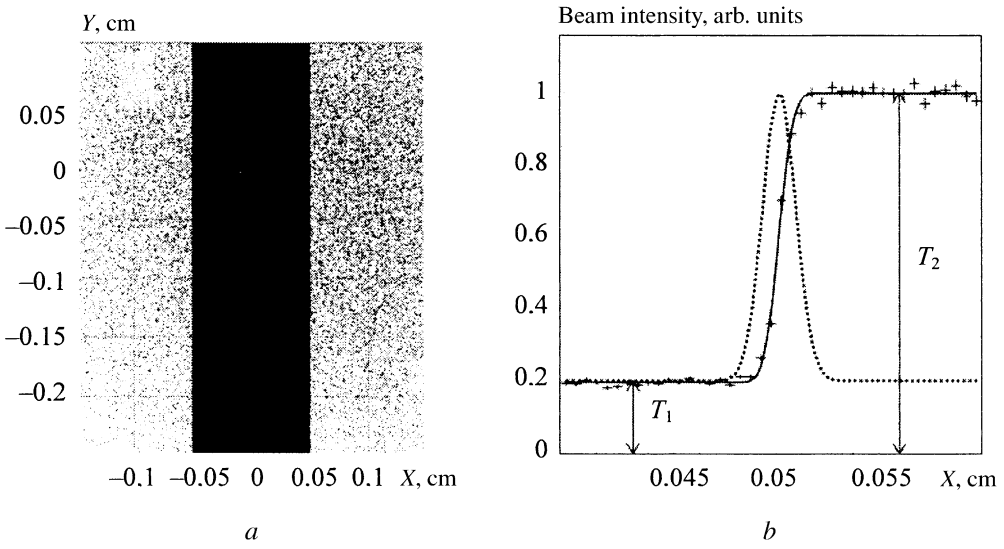

Fig. 4. Model of the test object "sharp boundary": *a*) simulation of the proton radiographic image for the system –1; *b*) horizontal profile of the right-hand boundary in the interval $-0.5 < y < 0.5$ (+) and results of fitting a Gaussian distribution (•).

the scintillation converters. In the simulation, it was assumed that the setup lies in a vacuum. The parameters of the initial proton beam were as follows: $p = 1.5$ GeV/sec, $\delta p/p = 0.1\%$, $\Delta\varphi = 0.5$ mrad.

The momentum and angular distributions of the protons relative to the axis of the beam on both sides of the OP, C, and IP planes (see Fig. 2) were constructed to check the correctness of the operation of the program and of the analysis of the effect of the components of the setup on the parameters of the proton beam. The evacuated volumes in the form of rectangular sheets were placed here. Entry of a proton into such volumes was detected by a special procedure performed in the GEANT program. The two-dimensional proton distribution in a plane perpendicular to the direction of the beam was taken as a model of the light image of the beam structure in this plane. To model the converter in the image plane, it was assumed that the converter operates in the proton counting mode, and the difference in the ionization losses of protons passing through different parts of the test objects was neglected. The number of channels of the two-dimensional distribution was chosen depending on the problem and the optical magnification coefficient of the system of lenses. As a rule, the number of channels was 1000×1000 for an image approximately 10 mm in size.

An important problem of numerical simulation of radiographic setups is finding the optimal choice of test objects whose metrological parameters can be estimated by analyzing their images. Two quantities were adopted to characterize the resolution of the radiographic setups numerically: the rms deviation of the normal distribution describing the image of the boundary between the components of test objects with different thickness and the number of line pairs at 1 mm which the setup can detect. The rms deviation was determined for a test object consisting of a 5 mm thick (along the beam axis) copper parallelepiped with transverse dimensions 1×3.5 mm.

Figure 4*a* shows the simulated image of a test object in the converter positioned in the IP plane. The distribution shown by the solid line in Fig. 4*b* is the profile of an image of the right-hand boundary of a parallelepiped on the abscissa in the range from –0.1 to 0.1 cm along the vertical direction. It is normalized to 1 in the region where the beam passes by the test object. The profile was approximated by the integral Gaussian distribution $T = a + b\Phi(x, x_0, \sigma)$, where a is the average intensity to the right of the flash, b is half the height of the flash, Φ is the integral Gaussian distribution function, and x_0 and σ are the average value and rms deviation of the distribution. The approximation gave the following parameters: $x_0 = 0.5 \pm 0.01$ mm and $\sigma = 8.1 \pm 0.5$ μm. The dotted line shows the differential Gaussian distribution whose parameters equal the numerical val-

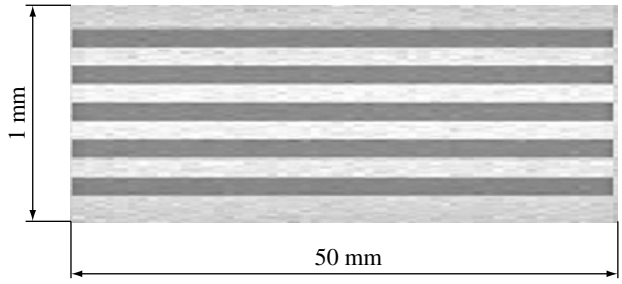

Fig. 5. Simulation of a proton radiographic image of a periodic 5 mm thick (in the beam direction) copper test structure. The image corresponds to five pairs of lines per 1 mm for the system −1.

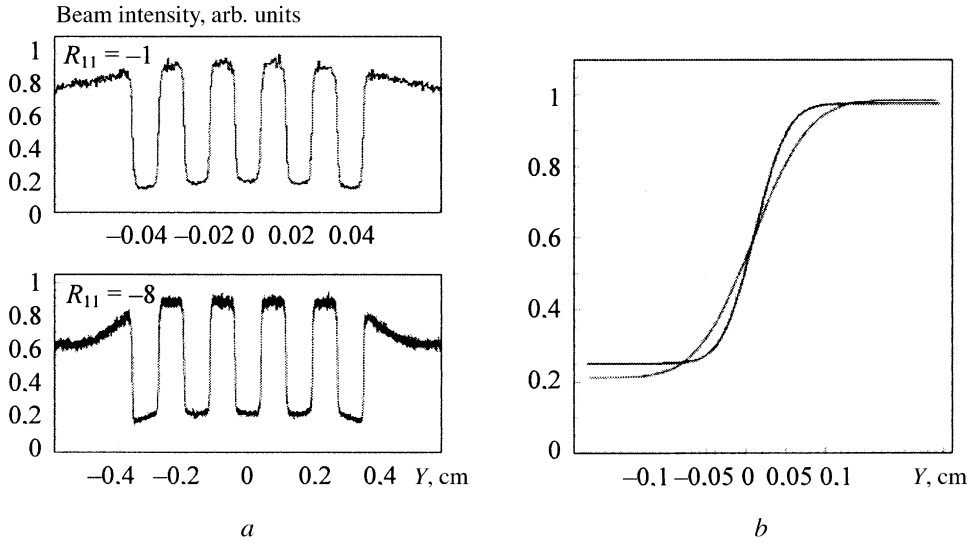

Fig. 6. Resolution of magnetic optics systems −8 and −1 of the setup for a periodic copper test object.

ues. The quantity σ is taken as a numerical estimate of the resolution of the radiographic setup, and $\eta = (T_2 - T_1)/(T_2 + T_1)$ is an estimate of the contrast (in our case $\eta = 0.67$). In the general case, the parameters σ and η depend on the shape and radiographic thickness of the test object.

The quantity L characterizing the capability of the setup to analyze periodic spatial structures is another parameter for estimating the resolution of the radiographic setup. It is expressed as the number of line pairs at 1 mm which the setup can resolve. A pair of lines is considered to be one period of the structure consisting of a signal–pause pair. Figure 5 shows a model image of a periodic structure with five pairs of lines at 1 mm being resolved; the structure was formed in a vacuum from 5 mm thick (in the direction of the beam) copper parallelepipeds with transverse dimensions 0.1×50 mm. The expected resolution of a real setup will not be worse than five pairs of lines per millimeter.

The resolution of a proton microscope (system −8) was estimated using a model of a periodic structure similar to the one shown in Fig. 5. Figure 6*a* compares the profiles of two-dimensional intensity distributions of protons detected in the image plane for two variants of the coefficient of magnification: the systems −1 and −8. The qualitatively better resolution of the microscope appears in the sharper boundaries of the troughs with $R_{11} = -8$. The contrast of the image is the same for both systems within the computational error. For a comparative quantitative assessment of the resolution, the integral normal distribution was fit to the right-hand boundary of the central dip. The microscope image was referenced to the object scale.

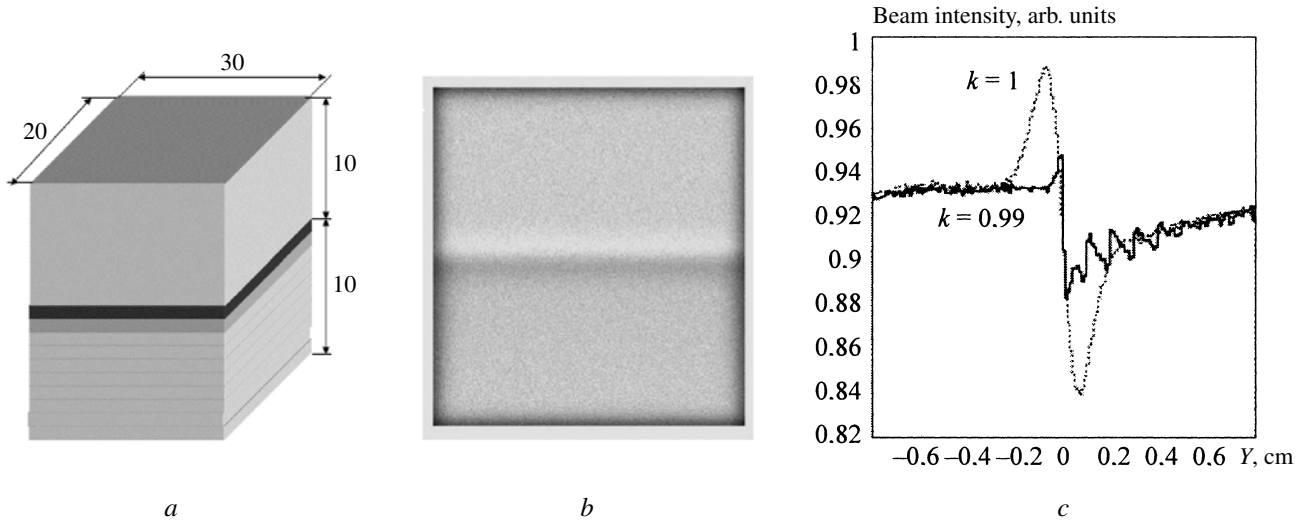

Fig. 7. Model of a detonation wave: *a*) simulation of a proton radiographic image for the system −1; *b*) image in the image plane; *c*) profile of the image along the vertical direction (k – correction factor for the magnetic field).

The following resolution was obtained: 7.8 μm for the system −1 and 4.6 μm for the proton microscope, respectively. The fitting functions in the scale of the object are presented in Fig. 6*b*.

Simulation of an Explosive Experiment. To prepare the proton radiography system for performing investigations in the physics of explosions, it is important to know its response in experiments investigating shock and detonation waves. Figure 7*a* shows a model constructed for a detonation wave on the basis of experimental results. It consists of 11 parallelepipeds made of a material simulating the chemical composition of an explosive but with a different density. The state of the explosive ~1 μsec after detonation is being simulated. The detonation is from below. For a detonation wave velocity ~10 km/sec, the front moves over a distance of about 10 mm. The density of the explosive is taken to be 1.8 g/cm^3, and the density of the detonation wave front is assumed to be 2.34 g/cm^3. The unloading zone is simulated with 10 plates, each 1 mm thick and with density decreasing from top to bottom with step 0.05 g/cm^3. The proton beam is moving from left to right.

The image of the model in the image plane is shown in Fig. 7*b*, and the profile in the vertical direction is shown in Fig. 7*c* (dotted line). The shock-wave front is oriented along the coordinate $Y = 0$, transverse to the beam axis. Negative values of Y in the figure represent the undetonated part of the explosive. A bipolar signal is observed near the front of the shock wave; such a signal is characteristic for proton radiographic images of the boundary of media with different radiographic thickness. In the unloading zone (in the region $Y > 0$), the intensity increases noticeably away from the front of the shock wave; this corresponds to a change in the density of the test object. The existence of a noise signal at $Y \cong 0$ distorts the real coordinate dependence of the density in the most interesting region. However, its effect can be decreased by readjusting the analyzing part of the magnetic channel. The solid line in the figure represents the profile of an image of the same object with the fields decreased by 1% in the lenses Nos. 4–7 simultaneously. In the absence of a noise signal, an adequate image is obtained in almost the entire region of observation.

In closing, we note that analysis of the metrological characteristics of the setup for proton radiography in the TWAC accelerator–storage complex shows that proton beams are promising for performing investigations in the physics of extreme states, in particular, for diagnostics of the dynamic properties of fast processes characteristic for shock and detonation waves.

This work was supported by the Federal Atomic Energy Agency under contracts N.4d.47.19.07.610 and N.4d.47.19.07.602, Grant 07-02-01396-a from the Russian Fund for Basic Research, and Grant HSh-1867.2003,2 “Leading Scientific Schools of the Russian Federation.”

REFERENCES

1. B. Sharkov, A. Golubev, and H. H. Hoffmann, "High-density plasma physics with heavy-ion beams," *Nucl. Instrum. Methods A*, **415**, No. 20, 20–26 (1998).
2. P. N. Alekseev, N. N. Alekseev, V. P. Zavodov, and A. D. Mil'yachenko, "Adiabatic trapping and acceleration of a beam in the booster synchrotron UK of the heavy-ion complex ITÉF-TVN," *Prib. Tekhk. Éksp.*, No. 4, 14–20 (2007).
3. A. Golubev, M. Basko, and A. Fertman, "Dense plasma diagnostics by fast proton beams," *Phys. Rev. E*, No. 57, pp. 3363–3367 (1998).
4. V. Mintsev, V. Gryaznov, and V. Fortov, "Stopping power of proton beam in a weakly nonideal xenon plasma," *Contributions to Plasma Phys.*, **39**, No. 1–2, 45–48 (1998).
5. A. F. Tulinov, V. S. Kuliskauskas, and M. M. Malov, "Proton scattering from a tungsten single crystal," *Phys. Lett.*, **18**, 304–307 (1965).
6. D. West and A. S. Sherwood, "Proton-scattering radiography," *Nondestructive Testing*, **6**, No. 5, 249–257 (1973).
7. B. A. Kononov and A. L. Lukin, *Proton Radiography*, Izd. Tomsk. Univer., Tomsk (1988).
8. A. V. Kantsyrev, N. V. Markov, A. A. Golubev, and V. S. Demidov, "Ion and proton radiography for static and dynamic experiments," in: *Scientific Session MIFI-2005*, pp. 80–81.
9. N. King, E. Ables, and K. Adams, "An 800-MeV proton radiography facility for dynamic experiments," *Nucl. Instrum. Methods A*, **424**, No. 94, 84–91 (1999).
10. V. S. Demidov et al., "Simulation of 0.8 GeV proton beam absorber," *Preprint ITÉF 1-05* (2005).
11. K. Makino and M. Berz, "COSY INFINITY. Version 9," *Nucl. Instrum. Methods A*, **558**, 346–350 (2005).
12. M. Szilagyi, *Electron and Ion Optics* [Russian translation], Mir, Moscow (1990).